

Light, Neutron, X-ray Scattering, and Conductivity Measurements on Aqueous Dodecyltrimethylammonium Bromide/1-Hexanol Solutions

Harald Preu,[†] Christine Schirmer,[†] Matija Tomšič,[‡] Marija Bešter Rogač,[‡] Andrej Jamnik,[‡] Luc Belloni,[§] and Werner Kunz^{*,†}

Institute of Physical and Theoretical Chemistry, University of Regensburg, D-93040 Regensburg, Germany, Faculty of Chemistry and Chemical Technology, University of Ljubljana, 1001-Ljubljana, Aškerčeva 5, Slovenia, and Service de Chimie Moléculaire, CEA/Saclay, F-91191 Gif-sur Yvette Cedex, France

Received: July 1, 2003; In Final Form: October 20, 2003

Ternary systems of dodecyltrimethylammonium bromide (C₁₂TAB)/1-hexanol/water are examined for series with constant surfactant to alcohol molar ratios of $n_s/n_a = 8:2, 8:4, 8:6$, and $8:8$ at surfactant concentrations of $c = 6.167\text{--}61.67\text{ g/L}$ ($0.02\text{--}0.20\text{ mol/L}$). The methods used are conductivity measurements, differential refractometry, static and dynamic light scattering, small-angle neutron scattering, and X-ray scattering. Critical micelle concentrations (cmc) and the degree of dissociation of the micelles are determined by conductivity measurements. The refractive index increment is given for each series as well as static and dynamic light-scattering intensities plotted as a function of the surfactant concentration. From small-angle neutron-scattering experiments a detailed picture of the size and the geometry of the micelles could be obtained, whereas small-angle X-ray scattering allowed information about the thickness of the interfacial film to be inferred. A hypernetted chain calculation with solvent plus ion-averaged screened Coulombic potentials combined with an ellipsoidal core/shell model permitted a simultaneous and coherent description of all scattering results.

1. Introduction

In practice, surfactants in aqueous solutions are frequently used in combination with one or several additives. These additives can change the micelle formation dramatically, and therefore, the properties of these mixtures can be modified and improved by changing the composition. Some widely used additives are inorganic salts, alcohols, and polymers. An increase of the ionic strength with the addition of inorganic salts favors micellar growth because of the screening effect of the charge of the hydrophilic headgroups, and changes of the geometrical shape toward ellipsoids and elongated structures may occur. The critical micelle concentration (cmc) is also influenced by the presence of additives.^{1,2}

The addition of alcohol can have different effects depending on the chain length of the alcohol. It is assumed that short and medium chain alcohols from methanol to 1-butanol can decrease the aggregation number of some surfactants in contrast to long chain alcohols such as 1-pentanol or 1-hexanol which may cause a decrease or increase of the micelle aggregation number depending on the concentration of alcohol and the type of surfactant.³ Because homogeneous and clear single phase surfactant solutions with alcohol contents much higher than the solubility in pure water can be prepared, these alcohols are often referred as cosurfactants which are incorporated into the micelles, and the solutions are called microemulsions.⁴

Numerous articles were published in recent years about cationic surfactants, especially about alkyltrimethylammonium bromides,^{5–11} and in many cases scattering techniques were used

to determine the structure of micellar aggregates. Especially at higher concentrations, small-angle scattering data were interpreted with the model of ellipsoidal micelles and with theoretically calculated structure factors.¹²

In the present paper we examine the influence of 1-hexanol on structural changes of dodecyltrimethylammonium bromide (C₁₂TAB) solutions that contain from 0.02 to 0.20 M of surfactant and up to equimolar concentrations of alcohol and surfactant (Figure 1). Our investigation is motivated by a parallel study of enzymatic activities in this system,¹³ which is an extension of our previous work on nonionic surfactant systems.^{14,15} In order to allow a deeper understanding of the enzymatic activities, structural information is required.

One might think that sufficient structural results are already known about C₁₂TAB/alcohol/water solutions or at least about the binary surfactant/water solutions. However, although many scattering results are known, there is still an ambiguity. For example, Bergström and Pedersen¹¹ argued that the micelles are far from spherical in shape, even at low concentrations. Part of the problem could be that often only one scattering method is used. In order to have a more unambiguous picture of the structure, we combined several different techniques and we tried to describe all of the data with a single model inferred from a statistical mechanics description.

2. Experimental Section

2.1. Materials. For our experiments we used the surfactant dodecyltrimethylammonium bromide (C₁₂TAB, purity $\geq 98\%$, Fluka, MW = 308.35 g/mol), 1-hexanol (C₆H₁₃OH, purity = 98%, Aldrich), and water (H₂O, deionized with a Millipore system, specific conductivity $\kappa \leq 10^{-7}\text{ }\Omega^{-1}\text{ cm}^{-1}$). For the small-angle neutron-scattering measurements we used deuterium oxide as solvent (D₂O, 99.9 atom% D, Aldrich). Stock solutions

* Authors to whom correspondence should be addressed. E-mail: werner.kunz@chemie.uni-regensburg.de.

[†] University of Regensburg.

[‡] University of Ljubljana.

[§] Service de Chimie Moléculaire.

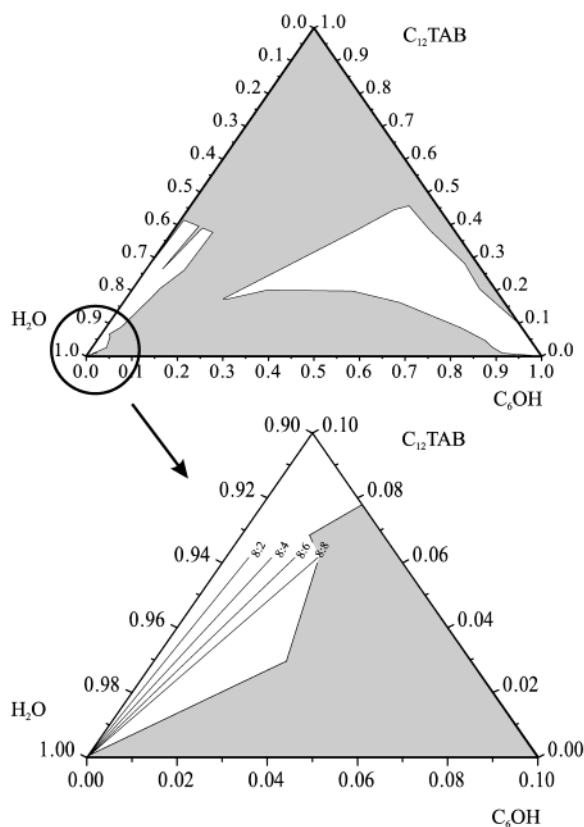


Figure 1. Ternary phase diagram of the system C₁₂TAB/1-hexanol/water at 25 °C, given in mass fraction. The gray areas indicate immiscible, and/or turbid, and/or inhomogeneous compositions. The straight lines marked with s82–s88 show the different paths of the investigated series. The path of s80 is on the left frame line.

were prepared by weighing, and the samples were made volumetrically.

2.2. Methods. Refractive indices were measured with a DR-1 differential refractometer from ALV (Langen, Germany) ($\lambda = 632.8$ nm, $T = (298.15 \pm 0.02)$ K, sensitivity $\pm 2 \times 10^{-6}$ refractive units) and a Hellma refractometer cell. The refractive index increment changes for different ratios of surfactant to alcohol and therefore has to be measured for every ratio.

The specific conductivities for the determination of the critical micellar concentrations were measured with a standard Consort C733 conductivity measurement device after calibrating the electrode with 0.01 M KCl ($T = (298.15 \pm 0.05)$ K). It is known that the addition of alcohol changes the cmc. Because of this, measurements were made with six different series of different compositions with a constant molar ratio of surfactant to alcohol, with each series consisting of 30 samples. The cmc was determined by linear-fitting of the points before and after the cmc region. The point of intersection of the two lines with different slopes gives the cmc.

Static (SLS) and dynamic (DLS) light-scattering experiments were carried out with a commercial goniometer (CGS-2, ALV) equipped with a vertical-polarized 22 mW HeNe laser (wavelength $\lambda = 632.8$ nm, $T = (298.15 \pm 0.01)$ K, homodyne mode), a fiber optical detection unit with an avalanche photodiode, and an ALV-5000/E multiple τ correlator. Cylindrical light-scattering cells (10 mm outer diameter, quartz suprasil) were purchased from Hellma and intensively cleaned in a five-step procedure to remove dust contamination. All solutions prepared for light scattering were filtered with a syringe filter with 200 nm pore size. To avoid concentration errors, the solutions were directly

filtered into the cells after pressing 2×2 mL of the solution through the filter. The cells were closed with Teflon stoppers and sealed with laboratory film. To determine the Rayleigh ratios R' of the samples, toluene as a standard and the solvent were measured. The Rayleigh ratio used for the toluene standard was $R'_{\text{st}} = 13.76 \times 10^{-4} \text{ m}^{-1}$ which was obtained by interpolation of different values given in the literature.^{16–19} The Rayleigh ratios and the diffusion coefficients of the samples were determined for seven angles θ from 60 to 120°, and no angular dependence was detected. The error of the average value is less than 2%.

The DLS measurements were performed by recording the average of at least 10 runs of the normalized intensity autocorrelation function $g_2(t)$ which is related to the normalized field correlation function $g_1(t)$ through the Siegert relation:

$$g_2(t) - 1 = \chi |g_1(t)|^2 \quad (1)$$

Here, χ is the coherence factor which is 1 in the case of an ideal measurement. For polydisperse solutions the measured diffusion coefficient D_m is related to $g_1(t)$ by the following:

$$|g_1(t)| = \int_0^\infty G(\Gamma) \exp(-\Gamma t) d\Gamma \quad (2)$$

$G(\Gamma)$ is the distribution function of the decay rates, $\Gamma = D_m q^2$, and $q = 4\pi/\lambda n_{\text{sol}} \sin(\theta/2)$, with n_{sol} being the refractive index of the solvent.

For the small-angle X-ray-scattering (SAXS) measurements, an evacuated high-flux SAXS instrument “SAXSess” (Anton Paar KG, Graz, Austria) was used. The modern focusing multilayer optics and the block-collimating unit of the SAXSess system produced an intense monochromatic primary beam. The camera was attached to a conventional X-ray generator equipped with a sealed X-ray tube (Cu anode target type, $\lambda_{\text{CuK}\alpha} = 0.154$ nm) operating at 40 kV and 50 mA. The samples were transferred to a standard quartz capillary for the SAXSess camera (with an outer diameter of 1 mm and a wall thickness of 10 μm) and placed in a thermally controlled sample holder, which was centered in the X-ray beam. The scattered X-ray intensities were measured with a 2D-imaging plate detection system (Fuji BAS1800 with Aida software from Raytest, Straubenhardt, Germany). The scattering intensity was sensed over the whole scattering range simultaneously with a spatial resolution of $50 \times 50 \mu\text{m}$ per pixel at a sample to detector distance of 265 mm. The measuring times that ensured reliable statistic were 60 min. For purposes of the numerical smearing procedure and the primary data treatment, the two primary beam cross-section profiles, water, and the empty capillary scattering were also measured. For the primary data treatment the program PDH from the program package PCG (Professor Otto Glatter, Institute of Chemistry, Graz, Austria) was used. The measured scattering intensities were put on an absolute scale using water as a secondary standard.²⁰

Small-angle neutron-scattering (SANS) experiments were performed at the PACE spectrometer at the Laboratoire Léon Brillouin (CEA-CNRS), CE-Saclay, France. Each sample was measured at two different wavelengths and detector positions ($\lambda_1 = 5.562$ Å, $d_1 = 1.2$ m and $\lambda_2 = 7.584$ Å, $d_2 = 3.0$ m) which covered a q -range from 0.008 to 0.298 Å^{-1} ($q = 4\pi/\lambda \sin(\theta/2)$, $T = (298.15 \pm 0.2)$ K), and $\Delta\lambda/\lambda$ was 0.10. The intensities were recorded at each run for 30 different angles simultaneously. To be able to calculate absolute intensities with the direct beam method in cm^{-1} , the scattering of the solvent was measured. Additional measurements of the transmission of

6 mm Plexiglas, graphite, and graphite in combination with 6 mm Plexiglas as attenuators were necessary. With the known detector geometry it was then possible to calculate the coherent differential scattering cross section of the sample.^{21,22} The background was taken into account by the application of the Porod law.²³

3. Theory

3.1. The HNC Calculation. We assumed that the micelles interact via a spherically symmetric solvent plus ion-averaged pair potential $u(r)$. We take for $u(r)$ the classical Derjaguin, Landau, Verwey, and Overbeek theory (DLVO) expression, which is the sum of the hard core and screened Coulombic contributions:²⁴

$$\beta u(r) = +\infty \quad r < 2a \quad (3)$$

$$= \frac{q_{\text{eff}}^2 L_B}{r} \frac{\exp[-\kappa(r - 2a)]}{(1 + \kappa a)^2} \quad r > 2a \quad (4)$$

where $\beta = 1/kT$ is the inverse temperature, a is the radius of the micelles, and $L_B = e^2/(4\pi\epsilon_0 kT)$ is the Bjerrum length (ϵ is the dielectric constant of the continuous solvent). As usual, the effective charge q_{eff} , which accounts for the ionic condensation, is lower than the structural value, equal to the aggregation number of the micelle N_{agg} . Last, the screening constant κ contains the contribution of the uncondensed counterions and of the salt ions. In the absence of added salt, the free monomers play the role of co-ions and the expression for κ reads (for monovalent ions):

$$\kappa = [4\pi L_B (2(\text{cmc}) + q_{\text{eff}} c_M)]^{1/2} \quad (5)$$

where $c_M = (c_{\text{monomer}} - \text{cmc})/N_{\text{agg}}$ is the number concentration of micelles.

From that pair potential, the pair distribution function $g(r)$ is calculated using the standard model of statistical mechanics of liquid, based on the Ornstein–Zernike (OZ) equation and the hypernetted chain (HNC) integral equation:

$$g(r) = \exp[-\beta u(r) + h(r) - c(r)] \quad (6)$$

Here, $h(r) = g(r) - 1$ and $c(r)$ represent the total and direct correlation functions, respectively. The HNC closure has been proven to be a good approximation for DLVO potentials in a wide domain of interaction parameters, and improved closures such as the Rogers–Young (RY) are unnecessary in the present study. After a numerical resolution of the OZ + HNC equations, one derives $g(r)$ and its equivalent in Fourier space, the static structure factor $S(q) = 1 + c_M \times \text{FT}(h)$.²⁴

3.2. Modeling of the SANS and SAXS Spectra. The coherent scattering contribution $I(q)$ due to solute particles results from interferences within and between particles. For the simplest case of spherical particles of radius a (and volume V) and homogeneous scattering length density s (s_0 for the solvent), the scattered intensity (in cm^{-1}) reads:

$$I(q) = c_M F^2(q) S(q) \quad (7)$$

where the amplitude factor of one isolated micelle $F(q)$ is given by

$$F(q) = (s - s_0) V 3 \frac{\sin(qa) - qa \cos(qa)}{(qa)^3} \equiv (s - s_0) V j_1(qa) \quad (8)$$

$F^2(q)$ is the form factor of the micelle.

In the present study, the micelles may become elongated, and we will use for the amplitude factor an ellipsoidal core/shell model with semiaxes a , a , b :²⁵

$$F^{\text{el.c/s}}(q) = (s^{\text{core}} - s^{\text{shell}}) V^{\text{core}} j_1(q \sqrt{a^{\text{core}2} \sin^2 \theta + b^{\text{core}2} \cos^2 \theta}) \quad (9)$$

$$+ (s^{\text{shell}} - s_0) V^{\text{shell}} j_1(q \sqrt{a^{\text{shell}2} \sin^2 \theta + b^{\text{shell}2} \cos^2 \theta}) \quad (10)$$

Here, θ represents the angle between the scattering vector \mathbf{q} and the principal axis of the ellipsoid.

Still assuming spherically symmetric interactions and correlations between particles in the solution, the scattered intensity becomes

$$I(q) = c_M (\langle F^{\text{el.c/s}2}(q) \rangle + \langle F^{\text{el.c/s}}(q) \rangle^2 (S(q) - 1)) \quad (11)$$

where the brackets $\langle \dots \rangle = \int_0^{\pi/2} \dots \sin \theta \, d\theta$ denote the average over the particle orientation θ .

In the case of neutron scattering, s^{core} is the averaged coherent scattering length density inside the core and is calculated as $s^{\text{core}} = (b^{\text{core}}/V^{\text{core}})$ in cm^{-2} , where b^{core} is the sum of the scattering lengths of the atoms in the core and $V^{\text{core}} = (4\pi/3)a^{\text{core}2}b^{\text{core}}$ (similar definitions exist for the shell). In the case of X-ray scattering, the s^i are derived from the local electron densities.

For strongly distorted ellipsoidal micelles, the assumption of spherically symmetric inter correlations may become questionable. Meanwhile, as long as the volume fraction of the hard objects remains low and the electrostatic interaction remains long range (no added salt), it has been shown that this approximation is valid and gives quantitatively correct results.²⁶

When creating a model of a micelle, one has to consider that the size of the micelles and their composition (the aggregation number and solvation of the polar part of the surfactant molecules and the alcohol partition coefficient) are not independent, and for the sake of consistency it is of course necessary that the number of free adjustable parameters be as small as possible.

For example, the size of the micelles must agree with the volume, which depends on the aggregation number and the penetration of solvent molecules into the micelles which together define the scattering length densities.

3.3. Static Light Scattering. The SLS results are usually given in terms of a Debye plot. In such a representation $K\Delta c/\Delta R'$ is plotted as a function of the surfactant concentration.

$$\Delta R' = R' - R'_{\text{cmc}}, \quad R' = \frac{I - I_{\text{solv}}}{I_{\text{st}}} R'_{\text{st}} \left(\frac{n_{\text{solv}}}{n_{\text{st}}} \right)^2 \quad (12)$$

$\Delta R'$ is the excess Rayleigh ratio of the aggregated surfactant. The Rayleigh ratio is calculated from the normalized scattering intensities I of the sample and of the solvent and standard, respectively, which are indicated by the subscripts “solv” and “st”. The refractive indices are given by n . In eq 12, R'_{cmc} was set to be the Rayleigh ratio at the cmc.²⁷

The optical constant K is defined as

$$K = \frac{4\pi^2 n_{\text{solv}}^2 (\partial n / \partial c)}{N_A \lambda^4} \quad (13)$$

where $(\partial n / \partial c)$ is the surfactant refractive index increment, $\lambda =$

632.8 nm is the wavelength, N_A is Avogadro's number, and Δc is the surfactant concentration c minus the cmc, in g/L.

In a straightforward data processing, the molecular weight of the scattering micelles can be determined by a virial expansion of $K\Delta c/\Delta R'^{28}$

$$\frac{K\Delta c}{\Delta R'} = \frac{1}{M_w} + B_s\Delta c + C_s\Delta c^2 \quad (14)$$

In eq 14, M_w is the weight-averaged molecular weight of the scatterer and B_s and C_s are virial coefficients. Note that in an SLS experiment, no extrapolation to zero-scattering angle is necessary, because $qa \ll 1$. The Rayleigh ratio is therefore proportional to the compressibility, which is in turn related to the structure factor at vanishing scattering angle, $S(0)$. This quantity is a result of the HNC calculation. The Debye plots should hence be correlated with the surfactant concentration dependence of $1/[M_w S(0)]$.

3.4. Dynamic Light Scattering. It is possible to calculate the concentration dependence of the mutual diffusion coefficient from the following expression:

$$D/D_0 = H(0)/S(0) \quad (15)$$

where D_0 is the ideal value obtained at vanishing micellar concentration and $H(0)$ represents the hydrodynamic interaction factor at $q = 0$.²⁹ In general, the hydrodynamic interactions between particles through the suspending medium are an N -body phenomenon and are not pairwise additive. Meanwhile, as long as the volume fraction occupied by the micelles which is at the origin of these indirect interactions remains low, it is usually sufficient to calculate $H(0)$ at the pair level. In that standard case, $H(0)$ is expressed as a simple integral of the pair mobility and pair distribution function $g(r)$ ³⁰

$$H(0) = 1 - 6.44c_M V + c_M \int_{2a}^{\infty} \left(\frac{a}{r} - \frac{5}{4} \left(\frac{a}{r} \right)^4 + \frac{9}{8} \left(\frac{a}{r} \right)^6 + \frac{25}{4} \left(\frac{a}{r} \right)^7 \right) (g(r) - 1) dr \quad (16)$$

Note that these expressions for the mutual diffusion coefficient of the micelles implicitly neglect the coupling between the micellar and ionic diffusions (assumption of infinite ionic mobility). The noninstantaneous diffusion of the small ions may slow the motion of small particles at low salinity.^{31,32}

4. Experimental Results

4.1. Conductivity Measurements. The investigated systems are labeled s80–s88, indicating the series with molar ratios of surfactant/1-hexanol $n_s/n_a = 8:0$ – $8:8$ (see Figure 1). The maximum surfactant concentrations are about 0.20 M (62 g/L).

The measured conductivity data are shown in Figure 2. The cmc values determined by the conductivity measurements are given in Table 1 and Figure 3, where the data are fitted with a polynomial of the order two. The quality of the cmc determination can be regarded as good, because 30 samples have been measured for every value and the results for s80 agree with those found in the literature.^{33–35,45}

An analysis of these data can be done according to Treiner and Mannebach,³⁶

$$\log\left(\frac{\text{cmc}_M}{\text{cmc}_{M,H}}\right) = K_M m_H \quad (17)$$

where cmc_M and $\text{cmc}_{M,H}$ are the critical micellar concentrations without and with alcohol, respectively, and m_H is the molality

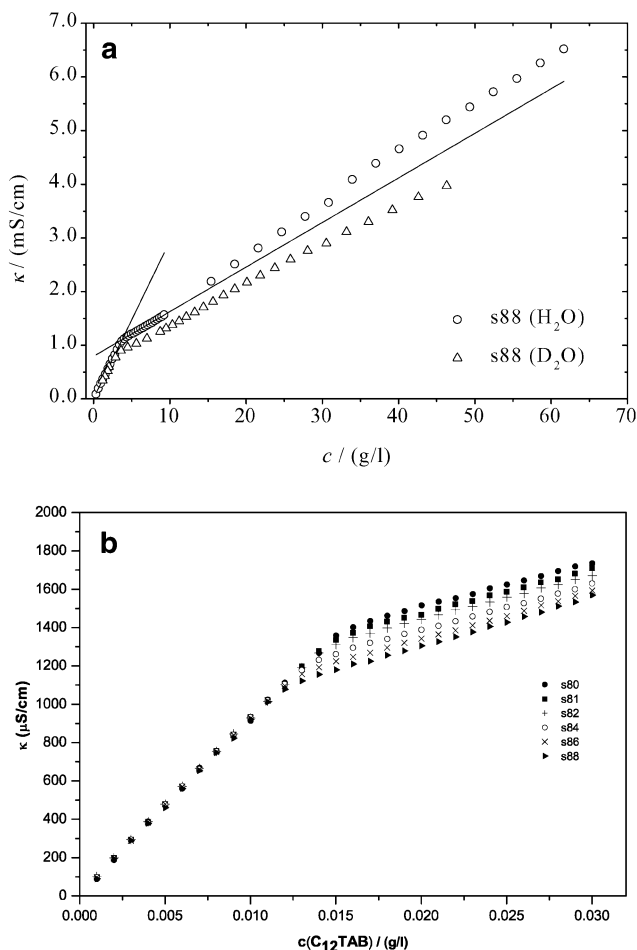


Figure 2. Specific conductivities κ as functions of the surfactant concentration. (a) Comparison between conductivities in normal and deuterated water. The linear fits indicate the cmc. The deviation of κ at higher concentrations from the straight line is due to structural changes of the micellar aggregates. For the series with D₂O as solvent, a smaller cmc and a slightly different behavior at higher concentrations is observed. (b) Conductivities of the series s80–s88 with different surfactant to alcohol ratios (cf. Section 4.1 and Table 1).

TABLE 1: Refractive Index Increment dn/dc , Degree of Ionization α , and Critical Micellar Concentrations cmc Inferred from Conductivity Measurements, Surfactant Aggregation Number N_{AG} from SLS, and Hydrodynamic Micellar Radius R_h from DLS^a

series	dn/dc (mL/g)	α	cmc (mL/g)	N_{AG}	R_h (g/L)	$S2/S1$
s80	0.1506	0.20	0.0153	52	16.0	0.25
s81			0.0147			0.25
s82	0.1615	0.20	0.0142	45	17.6	0.26
s84	0.1690	0.21	0.0132	45	18.4	0.26
s86	0.1770	0.20	0.0125	46	17.5	0.27
s88	0.1877	0.20	0.0121	47	19.0	0.28

^a N_{AG} and R_h are deduced from virial expansions (see text). Their numerical values are only valid close to the cmc. S1 and S2 are the slopes of the conductivity before and after the cmc (cf. Figure 2b).

of the alcohol. The K_M value obtained is $K_M = 8.0 \pm 0.5$ kg/mol, which is close to the literature value of $K_M = 7.9 \pm 0.25$ kg/mol.³⁶ As shown in refs 37 and 38, K_M can be split into a Setchenow coefficient and a partition coefficient.

The corresponding partition coefficient, as inferred by Treiner,³⁷ indicates that more than 80% of the alcohol is incorporated into the micelles. However, such a simple treatment of the cmc dependence on the cosurfactant concentration is only valid close to the cmc. In any case, it is expected that most of the 1-hexanol is in the micelles also at higher concentrations.

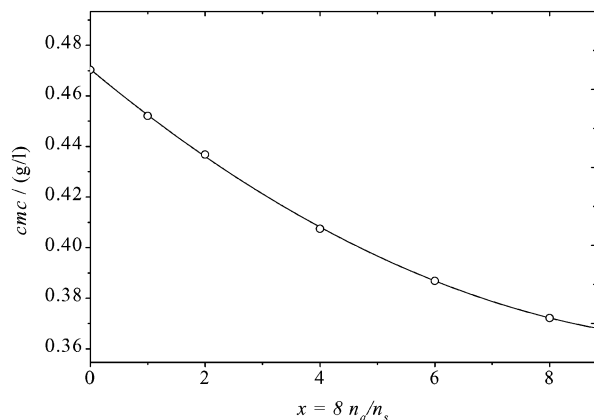


Figure 3. Critical micellar concentration cmc as a function of the molar ratio $n_s/n_a = 8/x$.

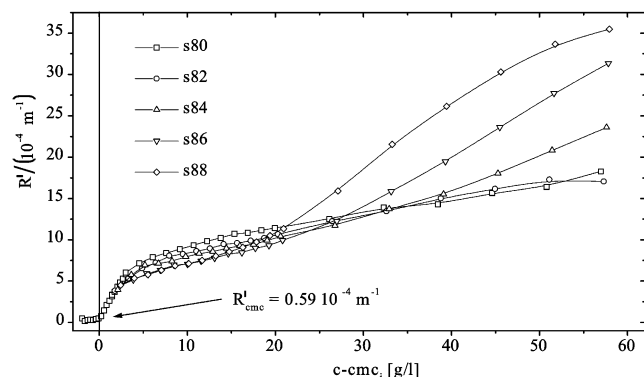


Figure 4. Rayleigh ratios of the series s80–s88. The full lines are to guide the eyes.

As will be discussed in Section 5, the scattering data are not sufficiently sensitive to give a quantitative value for the partition coefficients at various concentrations above the cmc. Therefore, for the sake of simplicity, a partition coefficient of 1 is used for the modeling of the spectra. In Figure 2a it can be seen that the cmc's depend on the isotopic state of the hydrogen atom. The value for the D₂O system is 2.894 g/L (9×10^{-3} M) compared to 3.731 g/L (1.21×10^{-2} M) for the equimolar surfactant–alcohol system in H₂O. This result must be considered for the HNC modeling of the SANS data, because it influences the number of micelles and free ions in the system.

Note that the slopes of the conductivity curves before and after the cmc are roughly independent of the different surfactant to hexanol ratios (see Figure 2b and Table 1).

4.2. Light Scattering. The SLS results of the investigated systems are given in Figures 4 and 5. Figure 4 shows the Rayleigh ratios R' as a function of the absolute surfactant concentration. At concentrations higher than 20 g/L, inflections can be observed for the series s84–s88. The sharp bend of the curve at low concentrations indicates the cmc and agrees with the value determined by conductivity measurements. The linear correlation coefficients of the fits (eq 14) are always better than 0.9992.

The measured diffusion coefficients D_m determined from dynamic light scattering are shown in Figure 6. The data were fitted with eq 18,

$$D_m = D_0 + B_d \Delta c + C_d \Delta c^2 \quad (18)$$

D_0 is the translational diffusion coefficient of the scattering particles, and B_d and C_d are coefficients which include hydro-

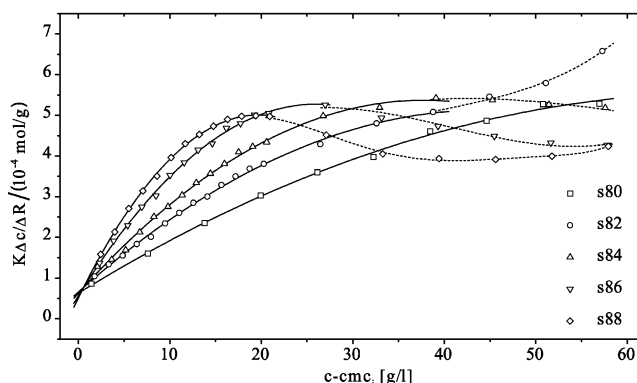


Figure 5. Debye plots of the series s80–s88. Full lines are quadratic fits, dashed lines are higher order fits to guide the eyes.

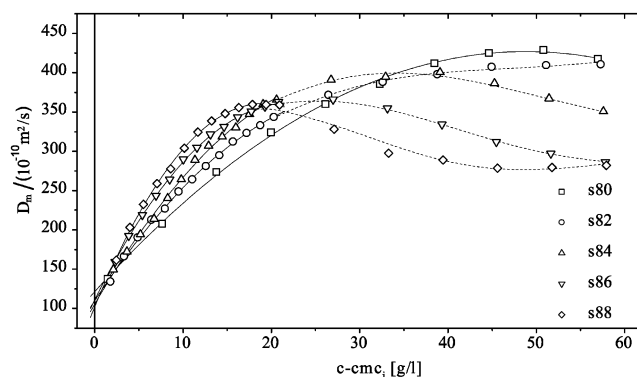


Figure 6. Measured diffusion coefficients as a function of concentration of the series s80–s88. Full lines are quadratic fits, dashed lines are higher order fits to guide the eyes.

dynamic and structural interactions. The hydrodynamic radii R_h listed in Table 1 are calculated with

$$D_0 = \frac{k_B T}{6\pi\eta R_h} \quad (19)$$

where $\eta_0 = 0.8902$ cP is the viscosity of the solvent which was assumed to be pure water. The diffusion coefficients D_m are obtained from a cumulant expansion of the correlation function which is recorded by the correlator.³⁹ The description of correlation functions of samples with possible polydispersity must be regarded as an approximation, but it gives, nevertheless, useful information. The quality of the DLS measurements themselves is good; the coherence factors χ are always high (>0.88). Furthermore, the results for the binary system are in very good agreement with a former DLS study.³²

4.3. SAXS and SANS. The HNC model calculations of SAXS spectra yield absolute scattering intensities, whereas the raw experimental SAXS data are not on an absolute scale. To compare the calculated and measured scattering functions, the absolute calibration of the latter was done using water as a secondary standard.²⁰ The geometric effects caused by the use of the slit collimation represent another problem. In this case the primary X-ray beam has finite dimensions with a nonhomogeneous intensity distribution, its shape being exactly described by its length and width cross-section profiles. This nonideal experimental design gives rise to the smearing effects on the ideal experimental scattering function described in detail in ref 40. For this reason, the scattering intensities that follow from the calculations using the HNC theory and a model for the form factor had to be numerically smeared by the measured

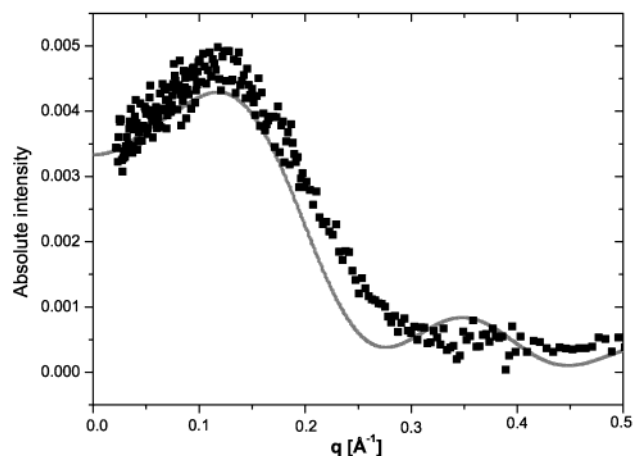


Figure 7. Experimental (squares) and calculated (line) SAXS spectra of the binary 0.0487 M C₁₂TAB solution in H₂O at 25 °C.

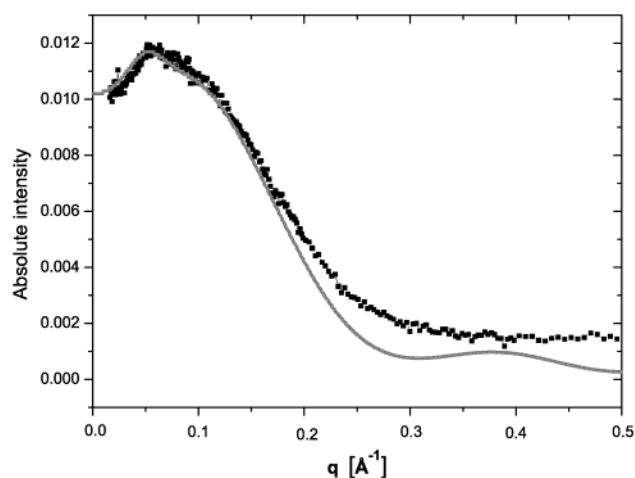


Figure 8. Experimental (squares) and calculated (line) SAXS spectra of the ternary solution of equimolar 0.0487 M C₁₂TAB and 1-hexanol in H₂O at 25 °C.

length and width cross-section profiles of the primary X-ray beam. The resulting smeared theoretical SAXS spectra could finally be compared to the smeared experimental data on an absolute scale. This comparison is made on Figures 7 and 8, where the experimental (squares) and theoretical (lines) SAXS spectra for two aqueous solutions, one containing 0.0487 M C₁₂TAB (Figure 7) and the other containing equimolar 0.0487 M C₁₂TAB and 1-hexanol (Figure 8), at 25 °C are displayed.

SANS data were recorded for three series of solutions in deuterated water. The surfactant concentrations range from 0.033 to 0.22 M for systems without 1-hexanol (Figure 9) and with 1-hexanol concentrations that are about half of the surfactant concentrations (Figure 10). For equimolar mixtures of C₁₂TAB and 1-hexanol, the corresponding concentrations are between 0.033 and 0.165 M (Figure 11). Note that 0.1 M C₁₂TAB corresponds to 30.8 g/L.

As stated earlier, the SANS experiments were made in D₂O to obtain a good contrast. With the substitution of the solvent, slight changes in the ternary phase diagram take place. For example, the sample with 61.67 g/L C₁₂TAB/1-hexanol/D₂O (series s88) is not homogeneous.

5. Data Analysis and Discussion

To get a consistent description of all of the scattering data, an HNC plus form factor modeling was undertaken. To do so, the description of the SANS data was the most convenient

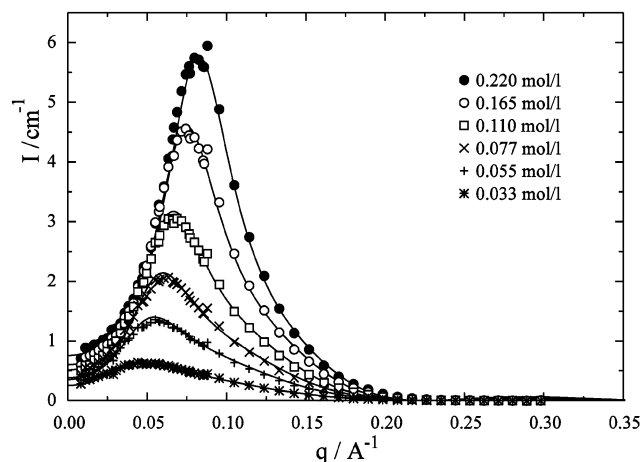


Figure 9. Experimental (symbols) and calculated (lines) SANS spectra of C₁₂TAB solutions in D₂O at 25 °C at different concentrations. The intensities *I* are given in absolute values.

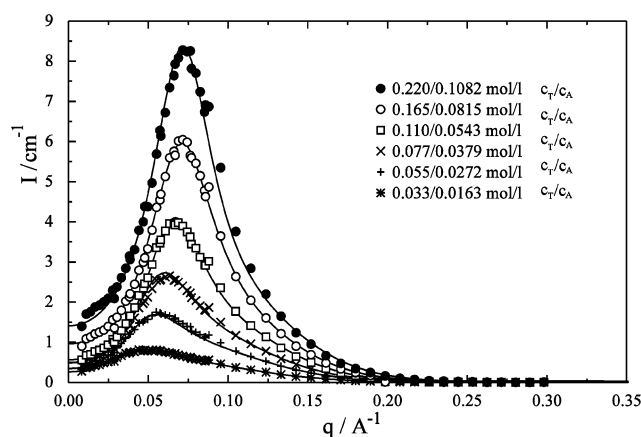


Figure 10. Experimental (symbols) and calculated (lines) SANS spectra of C₁₂TAB/1-hexanol solutions in D₂O at 25 °C at different concentrations. The molar ratio of surfactant/cosurfactant is 2:1.

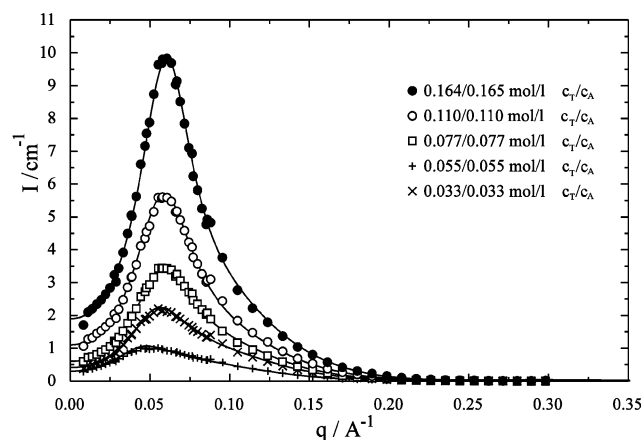


Figure 11. Experimental (symbols) and calculated (lines) SANS spectra of C₁₂TAB/1-hexanol solutions in D₂O at 25 °C at different concentrations. The molar ratio of surfactant/cosurfactant is 1:1.

starting point, because they contain information about both the forms of the objects and the interactions between them via the structure factors. Furthermore, 17 spectra were available.

Before the results are presented, we want to precisely explain what we mean by “modeling” and “fitting”. In contrast to other approaches such as the mean spherical approximation (MSA), HNC requires a numerical calculation, in which convergence is iteratively obtained. It would be extremely difficult if not

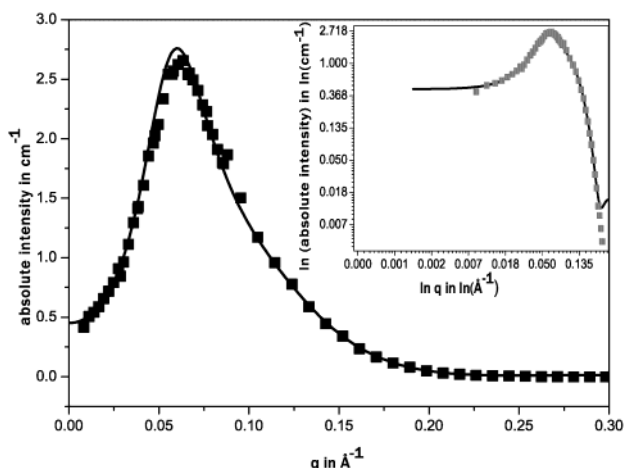


Figure 12. Typical fit of a SANS spectrum, obtained with HNC and a convenient form factor model.

impossible to make a weighted nonlinear least-squares fit of the spectra. Instead, our strategy was as usual:¹⁵ we chose a certain interaction potential and a reasonable form factor model, which should be in agreement with the potential model, at least as far as the overall size and the composition of the objects were concerned. Then we calculated the theoretical scattering curves and compared them to experimental data. We varied the potential and form factor parameters “by hand” until a reasonable agreement between theory and experiment was obtained. Of course, such a strategy did not guarantee that the “true” model was obtained; however, a comparison of the model for the SANS results with the experimental results of the other methods was a serious check for the validity of the model. Furthermore, some models could definitively be ruled out. For example, there was no way to get an agreement between theory and experiment with the assumption of oblate objects. Because a free variation of all three semi-axes of the ellipsoids did not bring a significant improvement of the data description, we always used the same values for at least two semi-axes. In principle, polydispersity should also be taken into account. That a certain size distribution is probable can be seen from the experimental scattering data, which are less structured than the theoretical curves. Polydispersity can be introduced in different ways.²⁶ In the present study, we considered mixtures of particles of different sizes and shapes. However, this procedure brought in a series of new adjustable parameters without significantly improving the data description. Therefore we renounced this approach and concentrated only on a monodisperse model.

Figure 12 shows a typical description of the experimental data. The adjusted parameters are the radius a of a sphere or the semi-axes $a_1 = a_2$ and b of a prolate object and the charge of the micelles. To have an idea of the effective micellar charge, a Poisson–Boltzmann calculation was performed prior to the HNC calculation.⁴¹ Furthermore, the scattering densities were estimated from the size of the objects and the scattering densities of C₁₂TAB, 1-hexanol, and deuterated water, assuming that all hexanol is within the micelles. The resulting scattering densities were in agreement with the measured absolute scattering intensities to within about 10%.

The values obtained from this modeling are summarized in Table 2.

That these values are also in agreement with the SAXS measurements can be seen from Figures 7 and 8, where experimental and calculated spectra are compared. Whereas the SANS data are essentially sensitive to the contrast between the micelles and the surrounding aqueous medium, the SAXS data

reflect the difference in electron density between the medium (intermediate electron density), the interface with the bromide counterions (high electron density), and the core of the micelles (low electron density).^{42,43} To get an agreement between the measured and the calculated SAXS spectra, the three different electron densities had to be adjusted. The thickness d of the interfacial layer was also a fitting parameter. The adjusted values are the following: (i) for the binary system $a = 18.4$ Å (inner core radius), $d = 2.1$ Å, the number of electrons per Å³ is 0.280 (core), 0.460 (shell), and 0.337 (continuous medium); (ii) for the ternary system $a = 15.5$ Å, $b = 25.9$ Å, $d = 2.1$ Å, the number of electrons per Å³ is 0.280 (core), 0.460 (shell), and 0.335 (continuous medium). Note that the electron densities are considered to be uniform within the three regions. The structure factors are the same as in the case of the SANS modeling. It should be stressed that the electron densities are very near to the theoretical ones inferred from the analytical and structural composition. Because the distribution of hexanol between the inside and the outside is not exactly known, the exact values are difficult to predict.

Initially, it was expected that the adjusted scattering density values could be used to quantify the partition of 1-hexanol between the micellar and the continuous phase. However, too many parameters influence this result, and so it can only be stated again that most of the alcohol is inside the micelles.

Figure 5 shows Debye plots of the systems investigated by SLS. The system s80 could be described over the whole concentration range using eq 14. The other systems were calculated up to concentrations where the sign of the slope or the sign of the curvature changes. The value for R'_{cmc} was determined experimentally. Figure 4 shows that it is reasonable to use R'_{cmc} as a constant for all series, because every series can be extrapolated into this point. The points of the series s80 are nearly constant at concentrations below the cmc. The obtained aggregation number of s80 agrees with those given in the literature.^{10,44}

The results are listed in Table 1. $N_{\text{AG}} = M_w/M_s$ is the aggregation number, where M_s is the molar weight of the surfactant monomer. Values of the specific refractive index increment (dn/dc) which are necessary for the calculation of the optical constant K are included, too.

The error of the determined aggregation number has to be evaluated critically. Rayleigh ratios given in the literature for pure liquids are afflicted with an error of at least 2%.^{16–18} In combination with the error of the measurement (which includes the error of the determination of dn/dc), it must increase. The determination of the cmc and of the value of R_{cmc} influences the result, too. Additionally, N_{AG} is obtained from an extrapolation, for which the real functional behavior is unknown. Furthermore, for the mixtures, N_{AG} is calculated assuming that all of the 1-hexanol is in the micelles. Therefore, it is obvious that N_{AG} cannot be determined with a precision higher than approximately 10–20%.

With known N_{AG} values, the degree of ionization $\alpha = p/N_{\text{AG}}$ is determined with the Evans equation (eq 20)⁴⁶ where p is the number of charges per micelle.

$$0 = [N_{\text{AG}}^{2/3}(S_1 - \lambda_{\text{Br}^-}^\infty)]\alpha^2 + \lambda_{\text{Br}^-}^\infty\alpha - S_2 \quad (20)$$

S_1 and S_2 are the slopes of the plots of the specific conductivity versus surfactant concentration before and after the cmc (see Figure 2b and Table 1). As can be seen from Table 1, α is independent of the fraction of alcohol. For the system s88 the conductivities were measured up to concentrations of 61.67 g/L. The α value for the series s80 is consistent with the literature.⁷

TABLE 2: Adjusted Values and Results of the HNC Calculations for the Description of the SANS Spectra^a

concentration (M)		cmc (M)	radius a (Å)	q_{eff}	N_{AG}	a (Å)	b (Å)	$D/D(0) = H/H(0)$	$S(0)$	$[S(0)M_w]^{-1}$
C ₁₂ TAB	hexanol									
0.033		0.012	19	18	74	19	19	2.2815	0.350	0.125
0.055		0.012	19.5	20	75	19.5	19.5	3.250	0.214	0.202
0.077		0.012	19.75	21	75	19.75	19.75	4.177	0.149	0.290
0.110		0.012	20	22	77	20	20	4.310	0.128	0.329
0.165		0.012	20	24	78	20	20	4.647	0.099	0.422
0.220		0.012	20	26	78	20	20	4.220	0.091	0.455
0.033	0.016	0.011	19.5	18	74	17.5	24	2.756	0.279	0.135
0.055	0.027	0.011	20	20	73	17.7	25	3.860	0.173	0.172
0.077	0.038	0.011	20.5	22	73	17.5	28	4.509	0.131	0.291
0.110	0.054	0.011	20.5	24	73	17.5	29	4.941	0.104	0.367
0.165	0.082	0.011	20.5	22	88	17.5	33	4.749	0.098	0.323
0.220	0.108	0.011	21.5	24	106	17.0	45	4.737	0.088	0.308
0.033	0.033	0.009	20	25	63	17.5	26	3.055	0.243	0.159
0.055	0.055	0.009	20.5	26	61	17.5	28	4.116	0.153	0.261
0.077	0.077	0.009	21.5	26	76	17.5	33	4.310	0.134	0.239
0.110	0.110	0.009	23.5	24	110	17.5	43	4.120	0.124	0.178
0.164	0.165	0.009	26.5	27	129	17.5	60	4.154	0.091	0.207

^a The variables a and q_{eff} are, respectively, the radius and the effective charge of the objects used for the charged hard-sphere potential and a and b are the radii of the prolate objects ($a = a_1 = a_2$) used to calculate the form factors. N_{AG} is the calculated aggregation number of the surfactants. $H/H(0)$, $D/D(0)$, and $S(0)$ are defined in the theoretical section. M_w is the weight-averaged molar mass of the micelles in kg/mol, calculated from the aggregation number and the molar masses of surfactant and hexanol and with the assumption that all of the hexanol, if present, is in the micellar phase.

The Debye plots are typical for micellar systems without added salt. At low micellar concentration ($q_{\text{eff}}c_M < \text{cmc}$) the osmotic pressure and hence the compressibility reflect the perfect gas pressure of the colloids only.²⁶ At high concentrations the Debye plots show a plateau, which is related to the perfect gas pressure of the free counterions and hence to the effective charge of the micelles.²⁶

From the last column of Table 2 it can be seen that the values of $1/[MS(0)]$ inferred from the HNC calculations and from the SANS experiments closely follow the Debye curves (cf. Section 3.3). However, the aggregation numbers deduced from the Debye fit are smaller than those inferred from the HNC calculations. Furthermore, the degree of ionization, $q_{\text{eff}}/N_{\text{AG}} = \alpha$, is between 0.25 and 0.30, instead of 0.2 as deduced from SLS.

The reasons for these discrepancies may be manifold. The Evans equation (eq 20) is the result of a very simplified model, and therefore, the differences in α are still acceptable. Because the exact composition of the micelles (e.g. the number of water molecules in them) is not known, it is difficult to convert M_w (SLS) to N_{AG} . Furthermore, M_w (SLS) is only valid close to the cmc, whereas the SANS spectra were recorded at higher surfactant concentrations. N_{AG} (HNC) is also rather indirectly determined. It is just used to estimate the number of micelles ($\Delta c/N_{\text{AG}}$). The scattering densities cannot be used for a precise determination of N_{AG} (HNC), because the molar volumes of the micelles and the micellar compositions are not exactly known. On the other hand, the HNC plus form factor description of the SANS and SAXS spectra is very sensitive to the size and shape of the micelles. Note that the structural results (sizes and shapes) obtained here are also in agreement with a recent SANS study of 0.3 M C₁₂TAB and of a mixture of 0.3 M C₁₂TAB and 0.1 M 1-hexanol.

For samples of the series s88 the plot of κ versus c shows slight deviations from the slope S_2 at concentration > 10 g/L (see Figure 2). In the literature,⁴⁵ those deviations are interpreted as a sign for structural changes and are discussed in terms of a second cmc. Such structural changes can well be explained by assuming a transition from spheres to prolate objects. However, at concentrations lower than 10 g/L no SANS spectrum was

recorded so that the spherical shape of micelles at that low concentration cannot be confirmed from the present study.

In the literature, it is discussed that a sphere-to-rod transition of C₁₂TAB takes place at 0.3 mol/L (92.5 g/L)⁴⁴ and at a temperature of 307.35 K a sphere-to-ellipsoid transition occurs at 32 mmol/L (9.87 g/L) as probed by ¹H NMR chemical shifts and relaxation rates measurements.⁴⁷ Both conditions are outside of the concentration and temperature range considered in the present paper, so no direct comparison can be made. However, it is somewhat surprising that Bergström and Pedersen found oblate micelles for C₁₂TAB at 40 °C.¹¹ According to their data processing, a small rise in temperature leads to oblate micelles, whereas additional cosurfactant, as regarded in our study, obviously results in prolate ones.

The hydrodynamic radii deduced from DLS are smaller than those expected by the SANS and SAXS results. In contrast, the change in the diffusion coefficients, as shown in Figure 6, is well reproduced by the $H/H(0)$ (HNC) results (cf. Table 2, ninth column). In particular, the maxima in the series s84 and s88 are in the right concentration range, and for the s88 series, even the second minimum is found. Consequently, significant changes in the hydrodynamic interactions with concentration do occur, despite the changes in the shape of the micelles. This is in agreement with a recent dielectric relaxation study on C₁₂TAB solutions.⁴⁸ It can be concluded that most of the results on C₁₂TAB and its mixtures with 1-hexanol, known from literature, could be confirmed in this study. The simultaneous description of SLS, DLS, SANS, SAXS, and conductivity results with the help of HNC and a convenient form factor gives a reliable picture of these systems. Nevertheless, ambiguity still persists as far as the aggregation numbers are concerned. The reason for this is that surfactant, cosurfactant, and water molecules are involved in the structuring, and each technique has a different sensitivity to these molecules. Our theoretical model does not take into account the granularity of the solvent and the detailed structure, for example, that in the shell layer of the micelles. Because a direct and simultaneous fit of the experimental data was not possible, the number of adjustable parameters had to be reduced in order to have a physically interpretable and unambiguous model. Polydispersity also cannot

be excluded. And finally, it is very difficult or even impossible to infer the micellar composition from the absolute scattering contrasts between the micellar phase and the bulk solution. So, care must be taken when scattering results are taken as the "true" picture of a complex solution. Nevertheless, the results are detailed enough to explain the basics of enzymatic solutions in these systems, as will be demonstrated in forthcoming papers.

Acknowledgment. The help of Dr. Julian Oberdisse and Dr. Loïc Auvray during the SANS experiment at the Laboratoire Léon Brillouin, (CEA-CNRS), CE-Saclay is gratefully acknowledged. We also thank Dr. Didier Touraud for useful discussions. M.T. thanks the Institute of Chemistry at the University of Graz. M.T. also thanks Professor O. Glatter and Dr. A. Bergmann for helpful discussions and Günther Scherf for technical assistance in performing the SAXS experiments. M.T., M.B.R., and A.J. acknowledge the support of the Ministry of Education, Science and Sport of Slovenia (Grants 0103-P-505 and 0103-P-506).

References and Notes

- (1) *Cationic Surfactants*; Rubingh, D. N., Holland, P. M., Eds.; Marcel Dekker: New York, 1991.
- (2) *Micelles, Membranes, Microemulsions, and Monolayers*; Gelbart, W. M., Ben-Shaul, A., Roux, D., Eds.; Springer-Verlag: Steinkopff Darmstadt, Germany, 1994.
- (3) Zana, R. *Adv. Colloid Interface Sci.* **1995**, *57*, 1.
- (4) Chevalier, Y.; Zemb, T. *Rep. Prog. Phys.* **1990**, *53*, 279.
- (5) Anacker, E. W.; Westwell, A. E. *J. Phys. Chem.* **1964**, *68*, 3490.
- (6) Jones, M. N.; Piercy, J. J. *Chem. Soc., Faraday Trans.* **1972**, *68*, 1839.
- (7) Zana, R. *J. Colloid Interface Sci.* **1980**, *78*, 330.
- (8) Imae, T.; Ikeda, S. *J. Phys. Chem.* **1986**, *90*, 5216.
- (9) Berr, S.; Jones, R. R. M.; Johnson, J. S., Jr. *J. Phys. Chem.* **1996**, *96*, 5611.
- (10) Aswal, V. K.; Goyal, P. S. *Physica B* **1998**, *245*, 73.
- (11) Bergström, M.; Pedersen, J. S. *Phys. Chem. Chem. Phys.* **1999**, *1*, 4437.
- (12) Santhanalakshmi, J.; Goyal, P. S.; Aswal, V. K.; Vijayalakshmi, G. *Proc. - Indian Acad. Sci., Chem. Sci.* **1999**, *111*, 651.
- (13) (a) Schirmer, C. Ph.D. Thesis, University of Regensburg, Regensburg, Germany, 2001. (b) Schirmer, C.; Kunz, W. University of Regensburg, Regensburg, Germany, to be submitted for publication.
- (14) Meziani, A.; Touraud, D.; Zradba, A.; Pulvin, S.; Pezron, I.; Clause, M.; Kunz, W. *J. Phys. Chem. B* **1997**, *101*, 3620.
- (15) Preu, H.; Zradba, A.; Rast, S.; Kunz, W.; Hardy, E.; Zeidler, M. D. *Phys. Chem. Chem. Phys.* **1999**, *1*, 3321.
- (16) Pike, E. R.; Pomeroy, W. R. W.; Vaughan, J. M. *J. Chem. Phys.* **1975**, *62*, 3188.
- (17) Moreels, E.; De Ceuninck, W.; Finsy, R. *J. Chem. Phys.* **1987**, *86*, 618.
- (18) Finnigan, J. A.; Jacobs, D. J. *Chem. Phys. Lett.* **1970**, *6*, 141.
- (19) Bender, T. M.; Lewis, R. J.; Pecora, R. *Macromolecules* **1986**, *19*, 244.
- (20) Orthaber, D.; Bergmann, A.; Glatter, O. *J. Appl. Crystallogr.* **2000**, *33*, 218.
- (21) Cotton, J. P. In *Neutron, X-ray and Light Scattering*; Lindner, P., Zemb, T., Eds.; Elsevier: Amsterdam, 1991.
- (22) Choi, S. M. SANS Experimental Methods. Presented at the NIST Center for Neutron Research Summer School, Gaithersburg, MD, June 2000.
- (23) Stradner, A.; Mayer, B.; Sottmann, T.; Hermetter, A.; Glatter, O. *J. Phys. Chem. B* **1999**, *103*, 6680.
- (24) Belloni, L. *J. Phys.: Condens. Matter* **2000**, *12*, R549.
- (25) Kotlarchyk, M.; Chen, S. H. *J. Chem. Phys.* **1983**, *79*, 2461.
- (26) Peyre, V.; Spalla, O.; Belloni, L.; Nabavi, M. *J. Colloid Interface Sci.* **1997**, *187*, 184.
- (27) Parfitt, G.; Wood, J. *Kolloid Z. Z. Polym.* **1969**, *55*, 229.
- (28) Annacker, E. W.; Westwell, A. E. *J. Phys. Chem.* **1966**, *70*, 2150.
- (29) Walrand, S.; Belloni, L.; Drifford, M. *J. Phys.* **1986**, *47*, 1565.
- (30) Corti, M.; Degiorgio, V. *J. Phys. Chem.* **1981**, *85*, 711.
- (31) Belloni, L.; Drifford, M. *J. Phys. (Paris) Lett.* **1985**, *46*, 1183.
- (32) Retailliau, P.; Riès-Kautt, M.; Ducruix, A.; Belloni, L.; Candau, S. J.; Munch, J. P. *Europhys. Lett.* **1999**, *46*, 154.
- (33) Kudryashov, E.; Kapustina, T.; Morrissey, S.; Buckin, V.; Dawson, K. J. *Colloid Interface Sci.* **1989**, *203*, 59.
- (34) Evans, D. F.; Allen, M.; Ninham, B. W.; Fouda, A. *J. Solution Chem.* **1984**, *13*, 87.
- (35) Moulik, S. P.; Haque, M. E.; Jana, P. K.; Das, A. R. *J. Phys. Chem.* **1996**, *100*, 701.
- (36) Treiner, C.; Mannebach, M. H. *J. Colloid Interface Sci.* **1987**, *118*, 244.
- (37) Treiner, C. In *Solubilization in Surfactant Aggregates*; Christian, S. D., Scamehorn, J. F., Eds.; Surfactant Science Series, Vol. 55; Marcel Dekker: New York, 1995; pp 383–428.
- (38) Marangoni, D. G.; Kwak, J. C. T. In *Solubilization in Surfactant Aggregates*; Christian, S. D., Scamehorn, J. F., Eds.; Surfactant Science Series, Vol. 55; Marcel Dekker: New York, 1995; pp 455–490.
- (39) Koppel, D. E. *J. Chem. Phys.* **1972**, *57*, 4814.
- (40) Glatter, O. In *Small Angle X-ray Scattering*; Glatter, O., Kratky, O., Eds.; Academic Press Inc. (London) Ltd.: London, 1983.
- (41) Alexander, S.; Chaikin, P. M.; Grant, P.; Morales, G. J.; Pincus, P.; Hone, D. *J. Chem. Phys.* **1984**, *80*, 5776.
- (42) Zemb, T.; Charpin, O. *J. Phys.* **1985**, *46*, 249.
- (43) Cecutti, C.; Focher, B.; Perly, B.; Zemb, T. *Langmuir* **1991**, *7*, 2580.
- (44) Brady, J. E.; Evans, D. F.; Warr, G. G.; Grieser, F.; Ninham, B. W. *J. Phys. Chem.* **1986**, *90*, 1853.
- (45) Pérez-Rodríguez, M.; Prieto, G.; Rega, C.; Varela, L. M.; Sarmiento, F.; Mosquera, V. *Langmuir* **1998**, *14*, 4422.
- (46) Evans, H. C. *J. Chem. Soc.* **1956**, *1*, 579.
- (47) Lee, Y. S.; Woo, K. W. *Bull. Korean Chem. Soc.* **1993**, *14*, 392.
- (48) Baar, C.; Buchner, R.; Kunz, W. *J. Phys. Chem. B* **2001**, *105*, 2914.